Scenario and Model Dependence of Strategic Solar Climate Intervention in CESM

J. T. Fasullo[1] and J. H. Richter[1]

[1]National Center for Atmospheric Research, Boulder, CO, 80301.

Corresponding author: Dr. John Fasullo (fasullo@ucar.edu)

Key Points:

- A substantial contrast in the meridional structure of stratospheric aerosols exists in two recent climate intervention experiments.
- The contrasts are found to be driven by a combination of model structural and scenario uncertainties.
- These uncertainties suggest the need for significant flexibility in geoengineering implementation.

Abstract

Model dependence in simulated responses to stratospheric aerosol injection (SAI) is a major uncertainty surrounding the potential implementation of this solar climate intervention strategy. We identify large differences in the aerosol mass distributions between two recently produced climate model SAI large ensembles, despite using similar climate targets, with the goal of understanding the drivers of such differences. Using a hierarchy of recently produced simulations, we identify three main contributors including: 1) the rapid adjustment of clouds and rainfall to elevated levels of carbon dioxide, 2) the associated low-frequency dynamical responses in the Atlantic Meridional Overturning Circulation, and 3) the contrasts in future climate forcing scenarios. Each contribution also represents a potentially irreducible uncertainty over the likely timeframe of a potential SAI deployment if a 1.5C target is to be met and the results thus suggest the need for significant flexibility in the deployment of SAI if enacted.

Plain Language Summary

The continued high levels of anthropogenic greenhouse gas emissions increase the likelihood that key climate warming thresholds will be exceeded in the coming decades unless some form of climate intervention is implemented. It is in this context that we examine a recently proposed approach to stratospheric aerosol injection (SAI). Using two recently produced climate model experiments, we find the associated latitudinal distribution of aerosol mass to exhibit substantial uncertainty, suggesting the need for significant flexibility in the location and amount of aerosol delivery. The uncertainty's origins relate to simulated climate responses to increases in carbon dioxide including rapid adjustments in clouds and the change in the overturning ocean circulation. Uncertainty in future anthropogenic emissions of industrial sulfate aerosols also contribute to SAI uncertainty.

1 Introduction

Solar climate intervention (SCI), or solar geoengineering, has been proposed as a means of reducing the adverse impacts of climate change via the artificial enhancement of Earth's albedo. One SCI method proposed to temporarily offset anthropogenic warming and associated impacts is stratospheric aerosol injection (SAI), which involves the delivery of aerosols or precursor gases into the stratosphere. A major uncertainty surrounding the enactment of SAI is the climate system response to both continued emissions of carbon dioxide and prolonged elevated levels of stratospheric sulfate aerosols.

It is in the context of this uncertainty that the National Academies of Sciences, Engineering, and Medicine (NASEM) recently called for further research to understand various SCI approaches (NASEM, 2021) as SAI has been shown, in principle, to be a method of global climate intervention capable of achieving various temperature-based targets (Tilmes et al. 2018, MacMartin et al. 2019, Simpson et al. 2019). However, there remain large uncertainties in associated climate responses and impacts (Fasullo et al. 2018, Kravitz and MacMartin 2020) and adverse effects have been identified involving the water cycle and circulations in the troposphere, stratosphere, and ocean (Tilmes et al. 2018, Kawatani et al. 2011, Watanabe and Kawatani 2012, Fasullo et al. 2018, Xu et al. 2020, Xie et al. 2021, Sun et al. 2020, Abiodun et al. 2021, Banerjee et al. 2021 Krishnamohan and Bala 2022).

Climate models are an essential tool for exploring the potential benefits and impacts of the broad range of proposed SAI approaches. They depict the interactions between multiple processes involved in the climate response and simulate impact-relevant fields. They also provide a process-based understanding of response mechanisms and timescales. Due to the large internal variability of the climate system, the evaluation of SAI approaches often requires climate model large ensembles (Deser et al., 2012, Kay et al. 2015, Maher et al. 2021) using Earth system models (ESMs) capable of accurately representing a diverse set of processes involving stratospheric and tropospheric dynamics and chemistry, and time-varying aerosol distributions, aspects that are well-represented in only a few currently available ESMs (Franke et al. 2021).

While some recent work has found broad consistency in simulated responses to simple SAI depictions, such as solar dimming (e.g. Kravitz et al. 2021, Visioni et al. 2021), this work identifies and explores substantial climate response dependencies to a more realistic SAI representation based on explicitly resolved stratospheric aerosol injections, their evolving aerosol size distributions, their interactions with dynamical, chemical, and hydrologic processes, and related couplings between the land, atmosphere, ocean, and cryosphere (MacMartin et al. 2017, Tilmes et al. 2018, Richter et al. 2022). We explore the origin of inter-model differences and their physical basis. The models, experiments, and methods used are described in Section 2. The spatial and temporal structure of injected aerosols and climate responses are presented and discussed in Section 3 while the broader consequences for the potential implementation of SAI, and suggestions for future work, are presented in Section 4.

2 Materials and Methods

2.1 Models

With the goal of explicitly representing the dynamical, chemical, and hydrological aspects of the climate response to SAI, this work uses versions 1 and 2 of the Community Earth System Model (CESM1, CESM2). Both versions can be run in so-called high-top and low-top atmospheric configurations. The CESM1 high-top configuration uses the Whole Atmosphere Community Climate Model, version 5 (CESM1-WACCM5, Mills et al., 2017) as its atmospheric component and the CESM2 uses WACCM6 (CESM2-WACCM6, Gettelman et al. 2019). For the atmosphere, CESM1-WACCM5 has zonal and meridional resolutions of 0.9° and 1.25°, respectively, with 70 vertical levels and a model top of 140 km. The configuration allows for a full representation of stratospheric dynamics and has extensive middle atmospheric chemistry, and is a key improvement upon earlier model generations and many current climate models (e.g., Ferraro et al., 2015). Tropospheric physics in WACCM5 are the same as in the lower top configuration, the Community Atmosphere Model version 5 (CAM5, Park et al. 2014), the atmospheric component of the CESM1 (Hurrell et al. 2013). CESM1-WACCM5 explicitly simulates sulfate aerosol concentrations and size distributions via the Modal Aerosol Module (MAM3; Mills et al., 2017). Associated responses in ozone concentrations have a beneficial impact on the stratospheric circulation and its biennial variability (Richter et al., 2017) and these have been shown to reduce the CO_2-driven midlatitude jets' poleward shift under present-day climate change (Chiodo and Polvani, 2019). Confidence in the representations of sulfate aerosol processes and their radiative effects are bolstered by the relatively close agreement that exists between simulated and observed radiative responses to the 1991 eruption of Mount Pinatubo (Mills et al., 2017). The ocean component of all models used in this study is the Parallel Ocean Program version 2 (POP2; Smith et al., 2010; Danabasoglu et al., 2012), which as uniform zonal resolution of 1.125°, and variable meridional resolution ranging from 0.27° in the tropics to 0.64° in the extratropical northern hemisphere. The model has 60 vertical levels with a uniform resolution of 10 m in the ocean's upper 160 m.

CESM2-WACCM6 incorporates various advances including fully interactive tropospheric chemistry and an interactive crop model. Tropospheric physics is the same as in the low-top configuration, the Community Atmosphere Model version 6 (CAM6), which is the atmospheric component of CESM2 (Danabasoglu et al. .2020). CAM6 uses the Cloud Layers Unified By Binormals (CLUBB; Golaz et al., 2002; Larson, 2017) unified turbulence scheme and the updated Morrison-Gettelman microphysics scheme (MG2; Gettelman and Morrison, 2015). Minor changes to POP2 are incorporated in CESM2-WACCM6 (Danabasoglu et al., 2020).

3 Climate Model Experiments

3.1 CESM1-WACCM5 Simulations

A summary of design characteristics for the simulations used here are given in Table 1. We use CESM1-WACCM5 SAI simulations that are a part of the Geoengineering Large Ensemble (GLENS, Tilmes et al., 2018). GLENS consists of two large ensemble of simulations: one without and one with SAI. Both ensembles use the Representative Concentration Pathway 8.5 (RCP85) emissions scenario for greenhouse gases. The baseline GLENS simulations consists of free running RCP85 simulations from 2005 through 2030 (17 members), with an additional 3 members continuing through 2100 (CESM1-WACCM5-RCP85). The second set of GLENS simulations, GLENS-SAI, utilizes strategically enacted SAI (following Kravitz et al. 2017), which consists of twenty members from 2020 to 2097 in which aerosol injections are specified to achieve stabilization of temperature targets at their mean 2020 conditions under RCP85. The targets include near-surface air temperature's global mean, equator-to-pole gradient, and inter-hemispheric gradient. The predefined injection latitudes for GLENS-SAI are 15^o and 30^o in each hemisphere and SO_2 is injected about 5 km above the tropopause, or approximately 25 and 23 km for the 15^o and 30^o sites, respectively, with an arbitrarily chosen longitude of 180^o (Tilmes et al. 2018). The initialization of GLENS-SAI is made from three distinct members of the RCP85 experiment, which itself branched from distinct historical-era simulations, thus providing a diversity of initialized ocean states. GLENS has been used in a range of contexts (Fasullo et al. 2018, Simpson et al. 2019, Pinto et al., 2020, Da-Allada et al, 2020).

3.2 CESM2-WACCM6 Simulations

As with GLENS, we use two sets of CESM2-WACCM6 experiments.The CESM2-WACCM6 baseline simulations used are from the Coupled Model Intercomparison Project version 6 (CMIP6, Eyring et al. 2016) and the Assessing Responses and Impacts of Solar climate intervention on the Earth system with Stratospheric Aerosol Injection project ARISE-SAI, Richter et al. 2022). These include the unmitigated CMIP6 SSP585 simulations, to allow for comparison with the RCP85 experiments in GLENS (Tilmes et al. 2020). The second experiment used is the SAI ensemble, with strategically placed sulfur dioxide injection to keep the global mean temperature at $\sim$ 1.5 C over preindustrial temperatures (ARISE-SAI-1.5, Richter et al. 2022). These simulations are from 2035 to 2069 and use the same target metrics as GLENS-SAI, but for the 2020-2039 time average in the unmitigated CESM2-WACCM6 baseline simulations, in contrast to GLENS-SAI where targets are based on the 2010 – 2030 time period. The injections are again at 15^o and 30 ^{o} in both hemispheres and at an arbitrarily chosen longitude of 180^o, as in GLENS-SAI, but occur lower in the stratosphere (approx. 21 km). ARISE-SAI-1.5 simulations use the moderate Shared Socioeconomic Pathway (SSP) scenario of SSP245 for its defacto future scenario (Burgess et al., 2020), a moderate scenario where "the world follows a path in which social, economic, and technological trends do not shift markedly from historical patterns" (O'Neill et al. 2016). The temperature targets for ARISE-SAI-1.5 are based on the same regional metrics as in GLENS and the simulations consist of a 10-member ensemble.

3.3 Additional Simulations

In order to get insight into the origin of contrasts between the above simulations, we use additional experiments. Below the stratosphere, CAM5 and CAM6 use physical representations of the climate system that are highly similar to their WACCM counterparts and thus provide a means of estimating the tropospheric origin of associated contrasts. Simulations used include the CESM1 (Kay et al. 2015) and CESM2 (Rodgers et al. 2021) large ensembles, and a 10-member ensemble of CESM2 that makes use of CMIP5 historical and RCP85 prescribed forcing agents, (CESM2-RCP85, Forster et al. 2013). Idealized experiments using CESM1 and CESM2 are also used in which CO_2 is quadruped in both fixed-SST (4xCO2AMIP) and coupled ocean (Abrupt4xCO_2) frameworks. The accompanying AMIP and pre-industrial coupled experiments are also used. Together, these simulations allow for the estimation of so-called "rapid adjustments" to CO_2 and these are found to provide important insight into contrasts between GLENS and ARISE.

4 Results

The yearly stratospheric aerosol mass injections specified in GLENS-SAI and ARISE-SAI-1.5 are shown in Figure 1, where we examine the common period of 2035 to 2069 (Table 1). The greater total emissions in GLENS-SAI than ARISE-SAI-1.5 are expected as they correspond to greater offset CO_2 concentrations in GLENS-SAI. However less expected is the large disparity in the latitudinal distribution of injections, with the vast majority of GLENS-SAI aerosols injected at 30°N and 30°S, with secondary injections at 15°N and negligible injections at 15°S. This contrasts starkly with ARISE-SAI-1.5, where injections occur overwhelmingly at 15°S, with much smaller emissions at 15°N and 30°S, and negligible injections at 30°N. These relative proportions and their contrasts are approximately constant from 2035 to 2069.

To explore the processes that may underlie the contrasts in Fig. 1, the structure of warming is examined in Figure 2. Warming in both CESM1-WACCM5-RCP85 and CESM2-WACCM6-SSP585 shows various features expected under anthropogenic climate change such as greater increases over land and polar regions (Fig. 2a, b). Differences between experiments are also clearly evident however, particularly in the northern hemisphere (NH) extratropics, where warming is stronger in CESM1-WACCM5-RCP85 and a strong cooling in the North Atlantic (NATL) is evident in CESM2-WACCM6-SSP585. Differencing the simulations (Fig. 2c) highlights this systematically weaker warming in the NH in CESM2-WACCM6-SSP585 and stronger warming in the southern hemisphere (SH) subtropics, particularly in the subtropical stratocumulus cloud deck regions in the eastern ocean basins. When the analogous difference is made for the CESM1-LE and CESM2-LE (Fig. 2d) a similar overall pattern emerges, albeit with somewhat weaker magnitudes in the extratropical NH and SH, suggesting a possible role for WACCM in driving the contrasts in these regions, though scenario contrasts may also play a role. The role of scenario can be estimated by examining differences between CESM2-RCP85 and CESM2-LE

(Fig. 2e). The persisting negative differences in the NH suggest that the contrast between SSP370 and RCP85 drives a component of the NH extratropical warming difference in Fig. 2d, the origin of which is explored further below and shown to also exist for SSP585 versus RCP85. Notably, various features of the unmitigated warming contrast between CESM1-WACCM5-RCP85 and CESM2-WACCM6-SSP585 are shared by the differences in SAI regional warming patterns (Fig. 2f), such as the elevated warming in the southern subtropics and NH midlatitude extratropics, and relative cooling in the NATL and NH subpolar regions, in ARISE-SAI-1.5 relative to GLENS-SAI.

Changes in top-of-atmosphere (TOA) absorbed solar radiation (FSNT) are strongly tied to patterns of warming. In unmitigated CESM1-WACCM5-RCP85 and CESM2-WACCM-SSP585 simulations (Fig. 3a, b) increases in FSNT are widespread, consistent with 21st century climate projections generally (Trenberth and Fasullo, 2009), however their difference (Fig. 3c) shows a strong positive correlation with contrasting patterns of warming as strong SH subtropical warming in CESM1-WACCM5-RCP85 is accompanied by disproportionate FSNT increases while enhanced NATL cooling is coincident with strong decreases. When the CESM1-LE and CESM2-LE are compared (Fig. 3d), a similar general pattern of FSNT differences exists, albeit weaker, again suggesting a potential contribution from WACCM or scenario contrasts. When the CESM2-LE is compared to CESM2-RCP85 a similar but weaker pattern of differences is evident, suggesting a modest but detectible role for the future scenario in driving contrasts between the simulations. The pattern of FSNT change beween ARISE-SAI-1.5 and GLENS-SAI contrasts generally with that of the unmitigated simulations and instead largely reflects the combined and complex influence of changes in clouds and SAI (Fig. 3f).

Contrasting warming patterns in the Atlantic Ocean are also suggestive of the involvement of an additional important component of the energy budget, the Atlantic Meridional Overturning Circulation (AMOC), which transports heat northward in the Atlantic and redistributes ocean mass and energy globally. Differences between the response in AMOC in our experiments are explored in Figure 4. Changes in the strength of the leading mode of AMOC (Fig. 4a) contrast considerably across the experiments. In GLENS-SAI, the intensity of AMOC increases and this drives an associated enhanced northward transport of heat into the NATL (Fasullo et al. 2018). The strengthening contrasts however with all other simulations considered here (Fig. 4a) and with unmitigated climate projections generally (Zhang et al. 2019, Xie et al. 2021), where AMOC typically weakens during the 21st century. A similar decrease in intensity is evident between ARISE-SAI-1.5 and the unmitigated CESM1-WACCM5-RCP85 and CESM2-WACCM-SSP585. A key driver of AMOC's leading mode is deep water formation in the NATL and in this region simulation of ocean density and salinity also differ substantially between the various experiments. In GLENS-SAI, the subpolar NATL becomes denser and more saline (Fig 4b, 4c) while the subtropical north Atlantic Ocean becomes less dense. These changes accompany increases in evaporation and a net negative surface freshwater flux, which

enhances salinity and density (Fasullo et al. 2018). In ARISE-SAI-1.5 the situation is reversed, with the subpolar NATL becoming substantially less dense and fresher, with associated reductions in evaporation (not shown). In ARISE-SAI-1.5, density reductions are evident in the Atlantic at all latitudes below 200 to 500 m due to warming (not shown) and salinity increases are evident south of 40N, patterns that contrast markedly with GLENS-SAI. Causal connections between salinity, density, and AMOC intensity can be complex however and will be discussed further below.

Various additional diagnostics provide important background for understand contrasts in our SAI experiments. In Fig. 3, a focus on changes in patterns of FSNT is motivated by its dominant contribution to the net TOA flux (Fig. S1). While changes in outgoing longwave radiation exist (Fig. S2), they can generally be viewed as responding to differences in warming, rather than driving them, as they are positively correlated to temperature anomalies and thus offset, in many cases, changes in FSNT. Understanding the origin of interhemispheric FSNT gradients is therefore critical. In this context the 4xCO2AMIP and Abrupt4xCO_2 simulations provide important insight as they demonstrate that responses in clouds to elevated levels of CO_2 differ considerably between CESM1 and CESM2 in a way that is consistent with the need for greater SH mitigated radiative heating in the ARISE-SAI-1.5 experiment. For example, in CESM2 the radiative (Fig. S3) and cloud amount (Fig. S4) responses to 4xCO2AMIP in the SH are -1.8 W m^{-2} and -1.3%, respectively, while in CESM1 they are near zero (0.0 W m^{-2} and -0.3%). Comparable interhemispheric contrasts exist in the first 5 years of Abrupt4xCO_2 experiments and these are sustained for several decades (Fig. S5), outweighing the slow responses to warming. This highlights a need to understand the sensitivity of the climate response directly to CO_2 if uncertainties in the implementation of SAI are to be reduced.

The sensitivity of AMOC to CO_2 and SAI also exists as a key uncertainty. Diagnosing individual drivers of AMOC in fully coupled simulations is extremely challenging given the diversity of thermal, saline, and dynamical processes that drive its changes (Zhang et al. 2019). Various changes are however simulated that are consistent with having an influence and these include the modulation of salinity in the NATL (Zhang et al. 2022), as in ARISE-SAI-1.5 a widespread freshening occurs in contrast to salinity increases simulated in GLENS-SAI (Fig. S6). A similar salinity contrast is also simulated between CESM2-WACCM-SSP585 and CESM1-WACCM5-RCP85, and between the CESM2-LE and CESM1-LE, suggesting that the contrast is endemic to CAM5 and CAM6 (Fig. S6). This possibility is supported further by changes in rainfall in 4xCO2AMIP CO_2 simulations, as CESM2 simulates systematically weaker reductions in rainfall in the northern extratropics than does CESM1 (Fig. S7), both over the Atlantic Ocean and over much of northern extratropical land where runoff can influence ocean salinity. While neither model simulates changes in rainfall that on their own would weaken AMOC, the potential to offset the elevated buoyancy driven by warming is suggested to differ considerably. While further attribution of AMOC changes likely requires additional targeted experiments, the results here

point to a potentially important role for rapid adjustments in the water cycle.

Lastly, a role for the future climate scenario is suggested by the differences between CESM2-LE and CESM2-RCP85 warming and radiation patterns, given the stronger NH warming and FSNT changes east of Asia in simulations using RCP85 (Figs. 2e, 3e, S1e, S2e, S6e). This hypothesis can be explored by examining changes in atmospheric sulfate burdens (Fig. S8), which differ significantly through the 2030-70 period between the experiments used. In general, simulations that use RCP85 emissions show stronger reductions in burdens than those that use SSP370 or SSP585 (Fig. S8). Given the strong cooling associated with the burdens via their impact on clouds, these differences consistute an anomalous NH warming contribution in the 21st C for RCP85-based experiments (Fig. S8c-e) and thus require additional NH SAI.

5 Discussion and Conclusions

The analysis of our climate intervention and complementary experiments highlights a fundamental and perhaps underappreciated contributor to uncertainties surrounding SAI, the rapid adjustments of the climate system to CO_2. Such adjustments include both the responses of patterns in cloud fields, which drive radiation contrasts between hemispheres, and precipitation, which can influence upper ocean salinity, density, and associated circulations and energy flows. As shown here, the simulation of rapid adjustments can vary considerably across models and resolving such inter-model discrepancies is thus critical in order to better constrain the design parameters of SAI if implemented in nature. Uncertainties in future scenarios must also be reduced, and progress along this front has been made in recent years with the identification of biases in prescribed CMIP6 emissions (e.g. Paulot et al. 2018, Wang et al. 2021). Nonetheless this raises the important issue that the latitude of SAI injections will depend explicitly on ambient anthropogenic emissions of sulfate aerosols and formulation of an SAI strategy should be accompanied by well-defined industrial emissions targets.

There are also important limits on the results shown here. First, they are based on only two climate models, and in many respects these models share physics that is central to the representation of SAI. A broader consideration of structural model uncertainty is therefore warranted and it is likely that key sources of uncertainty are not well-estimated in contrasts between our experiments. A need therefore exists for a broader multi-model effort to realistically depict SAI, and coordinate associated model development efforts, for the vast majority of climate models that currently cannot represent associated processes and fields. Observational efforts to monitor relevant fields and guide model development activities are also crucial if the inherent risks and uncertainties of SAI are to be understood, quanitified, and reduced to a point where SCI might become a promising risk-mitigation measure.

Acknowledgments

This material is based upon work supported by the National Center for Atmo-

spheric Research (NCAR), which is a major facility sponsored by the National Science Foundation (NSF) under Cooperative Agreement 1852977 and by SilverLining through its Safe Climate Research Initiative. The CESM project is supported primarily by the NSF. Computing and data storage resources, including the Cheyenne supercomputer (doi:10.5065/D6RX99HX), were provided by the Computational and Information Systems Laboratory (CISL) at NCAR. We thank all the scientists, software engineers, and administrators who contributed to the development of CESM2. JF was also supported by NASA Awards 80NSSC17K0565 and 80NSSC22K0046.

Availability Statement

All GLENS-SAI and CESM1-WACCM5-RCP85 simulations are available to the community via the Earth System Grid (see information at www.cesm.ucar .edu/projects/community-projects/GLENS/). Output from the CESM1-LE, CESM2-LE, CESM2-RCP85, CESM2-WACCM6-SSP585, simulations and ARISE-SAI-1.5 simulations is freely available the NCAR Climate Data Gateway at https://doi.org/10.26024/0cs0-ev98 and https://doi.org/10.5065/9kcn-9y79 respectively. CMIP6 data including CESM2-WACCM6-SSP585, 4xCO2AMIP, and 4xAbruptCO_2 simulations are available online (https://esgf-node.llnl.gov/projects/cmip6/).

Author Contributions

Conceptualization: J. T. Fasullo, J. H. Richter

Data curation: J. T. Fasullo, J. H. Richter

Formal analysis: J. T. Fasullo

Funding acquisition: J. H. Richter

Methodology: J. T. Fasullo, J. H. Richter

References

Abiodun, B. J., Odoulami, R. C., Sawadogo, W., Oloniyo, O. A., Abatan, A. A., New, M., ... & MacMartin, D. G. (2021), Potential impacts of stratospheric aerosol injection on drought risk managements over major river basins in Africa. *Climatic Change*, 169(3), 1-19, https://doi.org/10.1007/s10584-021-03268-w.

Banerjee, A., Butler, A. H., Polvani, L. M., Robock, A., Simpson, I. R., & Sun, L. (2021), Robust winter warming over Eurasia under stratospheric sulfate geoengineering–the role of stratospheric dynamics. *Atmospheric Chemistry and Physics*, *21*(9), 6985-6997, https://doi.org/10.5194/acp-21-6985-2021.

Burgess, M. G., J. Ritchie, J. Shapland & Pielke R. Jr. (2021), IPCC baseline scenarios have over-projected CO2 emissions and economic growth. Env. Res. Lett., 16, 014016, https://doi.org/10.1088/1748-9326/abcdd2.

Chiodo, G., & Polvani, L. M. (2019), The Response of the Ozone Layer to Quadrupled CO 2 Concentrations: Implications for Climate. Journal of climate, 32(22), 7629-7642, https://doi.org/10.1175/JCLI-D-19-0086.1.

Da-Allada, C. Y., Baloïtcha, E., Alamou, E. A., Awo, F. M., Bonou, F., Pomalegni, Y., ... & Irvine, P. J. (2020), Changes in west African summer monsoon precipitation under stratospheric aerosol geoengineering. *Earth's Future, 8(7)*, https://doi.org/10.1029/2020EF001595.

Danabasoglu, G., Bates, S. C., Briegleb, B. P., Jayne, S. R., Jochum, M., Large, W. G., ... & Yeager, S. G. (2012). The CCSM4 ocean component. Journal of Climate, 25(5), 1361-1389, https://doi.org/10.1175/JCLI-D-11-00091.1.

Danabasoglu, G., Lamarque, J. F., Bacmeister, J., Bailey, D. A., DuVivier, A. K., Edwards, J., ... & Strand, W. G. (2020), The community earth system model version 2 (CESM2). *Journal of Advances in Modeling Earth Systems*, 12(2), https://doi.org/10.1029/2019MS001916.

Deser, C., Phillips, A., Bourdette, V., & Teng, H. (2012), Uncertainty in climate change projections: the role of internal variability. *Climate dynamics*, 38(3), 527-546, https://doi.org/10.1007/s00382-010-0977-x.

Eyring, V., Bony, S., Meehl, G. A., Senior, C. A., Stevens, B., Stouffer, R. J., & Taylor, K. E. (2016). Overview of the Coupled Model Intercomparison Project Phase 6 (CMIP6) experimental design and organization. *Geoscientific Model Development, 9(5),* 1937-1958, https://doi.org/10.5194/gmd-9-1937-2016.

Fasullo, J. T., Tilmes, S., Richter, J. H., Kravitz, B., MacMartin, D. G., Mills, M. J., & Simpson, I. R. (2018), Persistent polar ocean warming in a strategically geoengineered climate. *Nature Geoscience*, 11(12), 910-914.

Ferraro, A. J., & Griffiths, H. G. (2016), Quantifying the temperature-independent effect of stratospheric aerosol geoengineering on global-mean precipitation in a multi-model ensemble. *Environmental Research Letters, 11*(3), https://doi.org/10.1088/1748-9326/11/3/034012.

Forster, P. M., Andrews, T., Good, P., Gregory, J. M., Jackson, L. S., & Zelinka, M. (2013), Evaluating adjusted forcing and model spread for historical and future scenarios in the CMIP5 generation of climate models. *Journal of Geophysical Research: Atmospheres, 118(3)*, 1139-1150, https://doi.org/10.1002/jgrd.50174

Franke, H., Niemeier, U., & Visioni, D. (2021), Differences in the quasi-biennial oscillation response to stratospheric aerosol modification depending on injection strategy and species. *Atmospheric Chemistry and Physics, 21(11)*, 8615-8635, https://doi.org/10.5194/acp-21-8615-2021.

Golaz, J.-C., Larson, V. E., & Cotton, W. R. (2002). A PDF-based model for boundary layer clouds. Part I: Method and model description. *Journal of the Atmospheric Sciences*, 59, 3540–3551, https://doi.org/10.1175/1520-0469(2002)059%3c3540:APBMFB%3e2.0.CO;2.

Hurrell, J. W., Holland, M. M., Gent, P. R., Ghan, S., Kay, J. E., Kushner, P. J., ... & Marshall, S. (2013), The community earth system model: a framework for collaborative research. *Bulletin of the American Meteorological Society, 94(9)*, 1339-1360, https://doi.org/10.1175/BAMS-D-12-00121.1.

Kawatani, Y., Hamilton, K., & Watanabe, S. (2011). The quasi-biennial oscillation in a double CO 2 climate. *Journal of the Atmospheric Sciences*, *68*(2), 265-283, https://doi.org/10.1175/2010JAS3623.1.

Kay, J. E., Deser, C., Phillips, A., Mai, A., Hannay, C., Strand, G., ... & Vertenstein, M. (2015). The Community Earth System Model (CESM) large ensemble project: A community resource for studying climate change in the presence of internal climate variability. *Bulletin of the American Meteorological Society*, *96*(8), 1333-1349, https://doi.org/.

Jackson, L. C., Biastoch, A., Buckley, M. W., Desbruyères, D. G., Frajka-Williams, E., Moat, B., & Robson, J. (2022), The evolution of the North Atlantic Meridional Overturning Circulation since 1980. *Nature Reviews Earth & Environment*, 1-14, https://doi.org/10.1038/s43017-022-00263-2.

Jones, A., Haywood, J. M., Jones, A. C., Tilmes, S., Kravitz, B., & Robock, A. (2021), North Atlantic Oscillation response in GeoMIP experiments G6solar and G6sulfur: why detailed modelling is needed for understanding regional implications of solar radiation management. *Atmospheric Chemistry and Physics*, 21(2), 1287-1304, https://doi.org/10.5194/acp-21-1287-2021.

Kravitz, B., MacMartin, D. G., Visioni, D., Boucher, O., Cole, J. N., Haywood, J., ... & Tilmes, S. (2021), Comparing different generations of idealized solar geoengineering simulations in the Geoengineering Model Intercomparison Project (GeoMIP). *Atmospheric Chemistry and Physics*, 21(6), 4231-4247, https://doi.org/10.5194/acp-21-4231-2021.

Kravitz, B., & MacMartin, D. G. (2020), Uncertainty and the basis for confidence in solar geoengineering research. *Nature Reviews Earth & Environment*, *1*(1), 64-75, https://doi.org/ 10.1038/s43017-019-0004-7.

Krishnamohan, K. S., & Bala, G. (2022), Sensitivity of tropical monsoon precipitation to the latitude of stratospheric aerosol injections. *Climate Dynamics, 1-18*, https://doi.org/10.1007/s00382-021-06121-z.

Larson, V. E., (2017). CLUBB-SILHS: A parameterization of subgrid variability in the atmosphere. arXiv:1711.03675v2 [physics.ao-ph].

MacMartin, D. G., Kravitz, B., Tilmes, S., Richter, J. H., Mills, M. J., Lamarque, J. F., ... & Vitt, F. (2017). The climate response to stratospheric aerosol geoengineering can be tailored using multiple injection locations. *Journal of Geophysical Research: Atmospheres*, *122*(23), 12-574, https://doi.org/10.1002/2017JD026868.

MacMartin, D. G., Wang, W., Kravitz, B., Tilmes, S., Richter, J. H., & Mills, M. J. (2019), Timescale for detecting the climate response to stratospheric aerosol

geoengineering. Journal of Geophysical Research: Atmospheres, 124, 1233–1247. https://doi.org/10.1029/2018JD028906.

Maher, N., Milinski, S., & Ludwig, R. (2021). Large ensemble climate model simulations: introduction, overview, and future prospects for utilising multiple types of large ensemble. *Earth System Dynamics*, *12*(2), 401-418, https://doi.org/10.5194/esd-12-401-2021.

Mills, M. J., Richter, J. H., Tilmes, S., Kravitz, B., MacMartin, D. G., Glanville, A. A., Tribbia J. T, Lamarque J-F., Vitt F., Schmidt A., Gettelman A., Hannay C., Bacmeister J. T., and Kinnison, D. E. (2017), Radiative and chemical response to interactive stratospheric sulfate aerosols in fully coupled CESM1(WACCM). *Journal of Geophysical Research: Atmospheres, 122*, 13,061– 13,078, https://doi.org/10.1002/2017JD027006.

National Academies of Sciences, Engineering, and Medicine. Reflecting Sunlight: Recommendations for Solar Geoengineering Research and Research Governance. Washington, DC: *The National Academies Press.*, https://doi.org/10.17226/25762, 2021.

Park, S., Bretherton, C. S., & Rasch, P. J. (2014), Integrating cloud processes in the Community Atmosphere Model, version 5. *Journal of Climate*, 27(18), 6821-6856, https://doi.org/10.1175/JCLI-D-14-00087.1.

O'Neill, B. C., Tebaldi, C., Van Vuuren, D. P., Eyring, V., Friedlingstein, P., Hurtt, G., Knutti R., Kriegler E., Lamarque J-F., Lowe J., Meehl G. A., Moss R., Riahi K., and Sanderson B. M., (2016) The Scenario Model Intercomparison Project (ScenarioMIP) for CMIP6. *Geoscientific Model Development*, 9(9), 3461–3482, https://doi.org/10.5194/gmd-9-3461-2016.

Park, S., Bretherton, C. S., & Rasch, P. J. (2014). Integrating cloud processes in the Community Atmosphere Model, version 5. *Journal of Climate*, *27*(18), 6821-6856, https://doi.org/10.1175/JCLI-D-14-00087.1.

Paulot, F., Paynter, D., Ginoux, P., Naik, V., & Horowitz, L. W. (2018). Changes in the aerosol direct radiative forcing from 2001 to 2015: observational constraints and regional mechanisms. *Atmospheric Chemistry and Physics, 18(17),* 13265-13281, https://doi.org/10.5194/acp-18-13265-2018.

Pinto, I., Jack, C., Lennard, C., Tilmes, S., & Odoulami, R. C. (2020), Africa's climate response to solar radiation management with stratospheric aerosol. *Geophysical Research Letters*, 47(2), e2019GL086047, https://doi.org/10.1029/2019GL086047.

Richter, J. H., Tilmes, S., Mills, M. J., Tribbia, J., Kravitz, B., MacMartin, D. G., Vitt, F., and Lamarque J-F. (2017), Stratospheric dynamical response and ozone feedbacks in the presence of SO2 injections. *Journal of Geophysical Research: Atmospheres, 122*, 12,557–12,573, https://doi.org/10.1002/2017JD026912.

Richter, J., D Visioni , D G. MacMartin , D A. Bailey , N. Rosenbloom , W. R. Lee , M. Tye , & Lamarque, J-F (2022), ARISE Assessing Responses and Impacts of Solar climate intervention on the Earth system with stratospheric aerosol injection (ARISE-SAI), *Geoscientific Model Development.*, submitted.

Rodgers, K. B., Lee, S. S., Rosenbloom, N., Timmermann, A., Danabasoglu, G., Deser, C., ... & Yeager, S. G. (2021), Ubiquity of human-induced changes in climate variability. *Earth System Dynamics*, *12*(4), 1393-1411, https://doi.org/10.5194/esd-12-1393-2021.

Simpson, I. R., Tilmes, S., Richter, J. H., Kravitz, B., MacMartin, D. G., Mills, M. J., Fasullo J. T., and Pendergrass A. G. (2019), The regional hydroclimate response to stratospheric sulfate geoengineering and the role of stratospheric heating. *Journal of Geophysical Research: Atmospheres*, 124, 12587– 12616, https://doi.org/10.1029/2019JD031093.

Smith, W., & Wagner, G. (2018), Stratospheric aerosol injection tactics and costs in the first 15 years of deployment. *Environmental Research Letters*, 13(12), 124001, https://doi.org/10.1088/1748-9326/aae98d.

Smith, R., Jones P., Briegleb B., Bryan F., Danabasoglu G., Dennis J., Dukowicz J., Eden C., Fox-Kemper B., Gent P., Hecht M., Jayne S., Jochum M., Large W., Lindsay K., Maltrud M., Norton N., Peacock S., Vertenstein M., Year S. (2010), The Parallel Ocean Program (POP) reference manual, Ocean component of the Community Climate System Model (CCSM), LANL Technical Report, LAUR-10-01853, 141 pp.

Sun, W., Wang, B., Chen, D., Gao, C., Lu, G., & Liu, J. (2020), Global monsoon response to tropical and Arctic stratospheric aerosol injection. *Climate Dynamics, 55(7)*, 2107-2121, https://doi.org/10.1007/s00382-020-05371-7.

Tilmes, S., Richter, J. H., Kravitz, B., MacMartin, D. G., Mills, M. J., Simpson, I. R., ... & Ghosh, S. (2018), CESM1 (WACCM) stratospheric aerosol geoengineering large ensemble project. *Bulletin of the American Meteorological Society*, 99(11), 2361-2371, https://doi.org/10.1175/BAMS-D-17-0267.1.

Tilmes, S., MacMartin, D. G., Lenaerts, J., Van Kampenhout, L., Muntjewerf, L., Xia, L., ... & Robock, A. (2020), Reaching 1.5 and 2.0 C global surface temperature targets using stratospheric aerosol geoengineering. *Earth System Dynamics, 11(3),* 579-601, https://doi.org/10.5194/esd-11-579-2020.

Visioni, D., MacMartin, D. G., Kravitz, B., Boucher, O., Jones, A., Lurton, T., ... & Tilmes, S. (2021), Identifying the sources of uncertainty in climate model simulations of solar radiation modification with the G6sulfur and G6solar Geoengineering Model Intercomparison Project (GeoMIP) simulations. *Atmospheric Chemistry and Physics, 21(13),* 10039-10063, https://doi.org/10.5194/acp-21-10039-2021.

Wang, Z., Lin, L., Xu, Y., Che, H., Zhang, X., Zhang, H., ... & Xie, B. (2021). Incorrect Asian aerosols affecting the attribution and projection of regional cli-

mate change in CMIP6 models. *NPJ Climate and Atmospheric Science*, *4*(1), 1-8, https://doi.org/10.1038/s41612-020-00159-2.

Xie, M., Moore, J. C., Zhao, L., Wolovick, M., & Muri, H. (2021), Impacts of three types of solar geoengineering on the North Atlantic Meridional Overturning Circulation. *Atmospheric Chemistry and Physics Discussions*, 1-28, https://doi.org/10.5194/acp-2021-877.

Xu, Y., Lin, L., Tilmes, S., Dagon, K., Xia, L., Diao, C., ... & Burnell, L. (2020), Climate engineering to mitigate the projected 21st-century terrestrial drying of the Americas: Carbon Capture vs. Sulfur Injection. *Earth System Dynamics*, https://doi.org/10.5194/esd-2020-2.

Zhang, R. R. Sutton, G. Danabasoglu, Y.-O. Kwon, R. Marsh, S. G. Yeager, D. E. Amrhein, C. M. Little, (2019), A review of the role of the Atlantic meridional overturning circulation in Atlantic multidecadal variability and associated climate impacts. *Rev. Geophys.* **57**, 316–375 (2019), https://doi.org/10.1029/2019RG000644.

Zhang, Q., Chang, P., Yeager, S. G., Danabasoglu, G., & Zhang, S. (2022), Role of sea-surface salinity in simulating historical decadal variations of Atlantic meridional overturning circulation in a coupled climate model. *Geophysical Research Letters*, 49, e2021GL096922. https://doi.org/10.1029/2021GL096922.

Zhao, M., Cao, L., Bala, G., & Duan, L. (2021), Climate response to latitudinal and altitudinal distribution of stratospheric sulfate aerosols. *Journal of Geophysical Research: Atmospheres, 126*, e2021JD035379. https://doi.org/10.1029/2021JD035379

Table 1. Climate model experiments used in this study and their design characteristics.

Ensemble Name	Lateral Resolution	Vertical Levels	# mem	Time Span	Future Scen
CESM1-WACCM5-RCP85	0.9ºx1.25º	70	20 (3*)	2006-2030 (2099)	RCP85
GLENS-SAI	0.9ºx1.25º	70	20	2020-2097	RCP85+SA
CESM2-WACCM6-SSP585	0.9ºx1.25º	70	5		SSP585
ARISE-SAI-1.5	0.9ºx1.25º	70	10	2035-2069	SSP245+SA
CESM1-LE	0.9ºx1.25º	30	40	1920-2100	RCP85
CESM2-LE	0.9ºx1.25º	32	50	1850-2100	SSP370
CESM2-RCP85	0.9ºx1.25º	32	10	1920-2100	RCP85
CESM1-AMIP	0.9ºx1.25º	30	1	1979-2005	N/A
CESM1-4xCO2AMIP	0.9ºx1.25º	30	1	1979-2005	N/A
CESM2-AMIP	0.9ºx1.25º	32	1	1979-2014	N/A
CESM2-4xCO2AMIP	0.9ºx1.25º	32	1	1979-2014	N/A
CESM1-PI	0.9ºx1.25º	30	1	0-1800	N/A
CESM2-PI	0.9ºx1.25º	30	1	0-2000	N/A
CESM1-Abrupt4xCO2	0.9ºx1.25º	32	1	0-150	N/A
CESM2-Abrupt4xCO2	0.9ºx1.25º	32	1	0-150	N/A

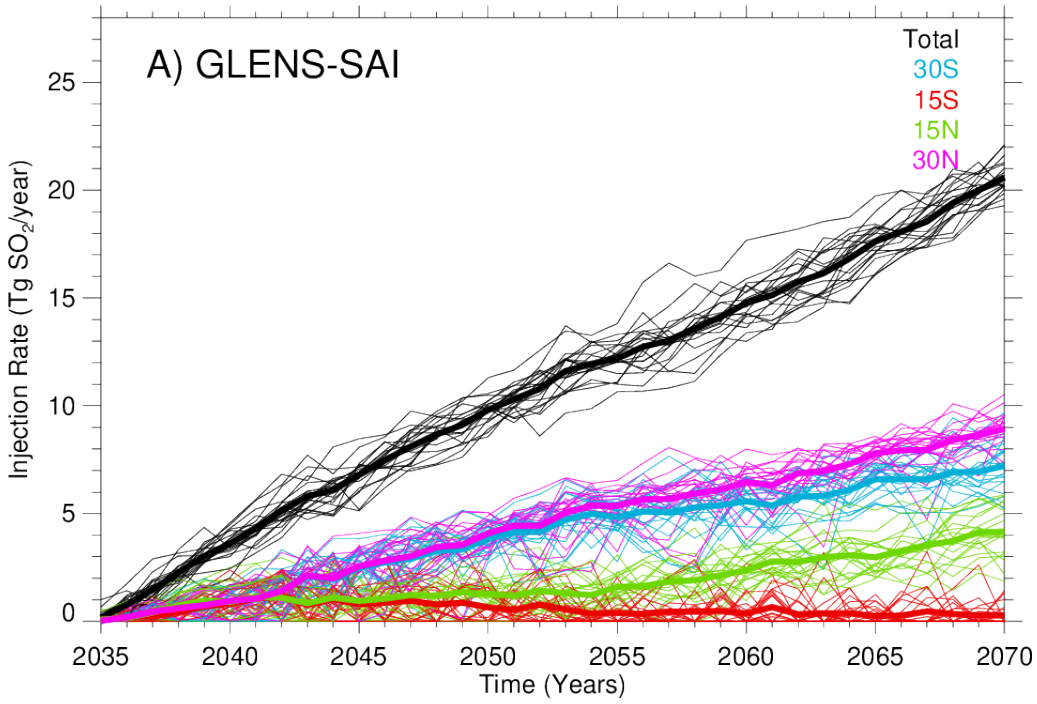
A) GLENS-SAI
Total
30S
15S
15N
30N
Injection Rate (Tg SO2/year)
0
5
10
15
20
25
2035
2040
2045
2050
2055
2060
2065
2070
Time (Years)

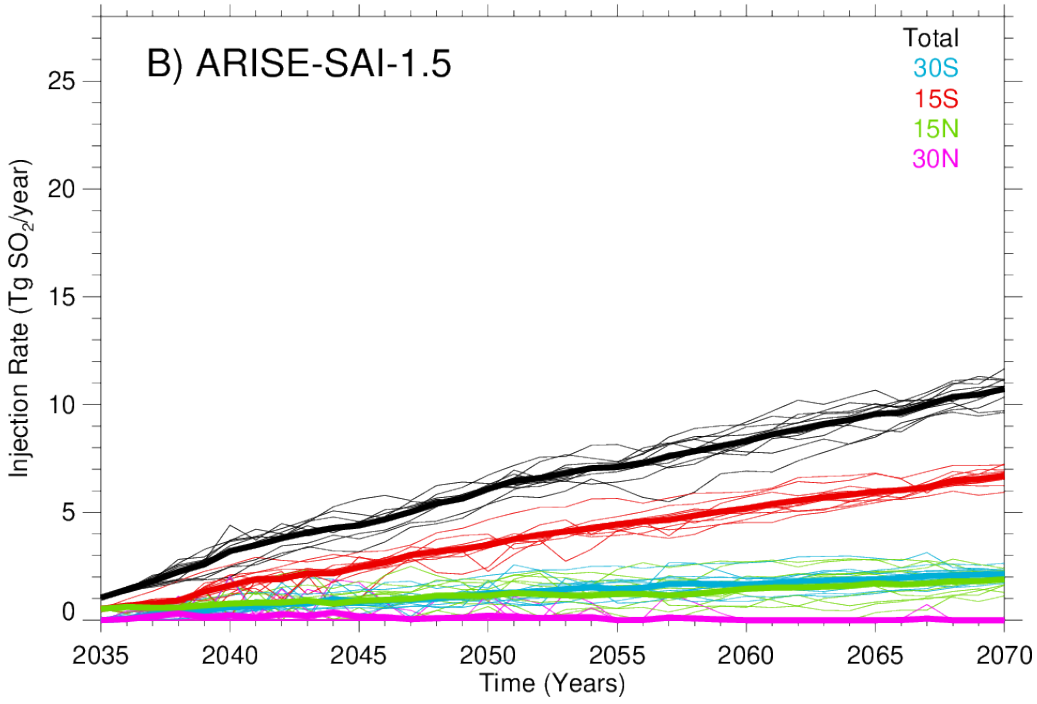
B) ARISE-SAI-1.5
Total
30S
15S
15N
30N
Injection Rate (Tg SO2/year)
0
5
10
15
20
25
2035
2040
2045
2050
2055
2060
2065
2070
Time (Years)

Figure 1. Evolution of yearly sulfur dioxide injections (Tg SO_2 yr^{-1}) over time at the four injection latitudes for (a) GLENS-SAI and (b) ARISE-SAI-1.5 from 2035 to 2070.

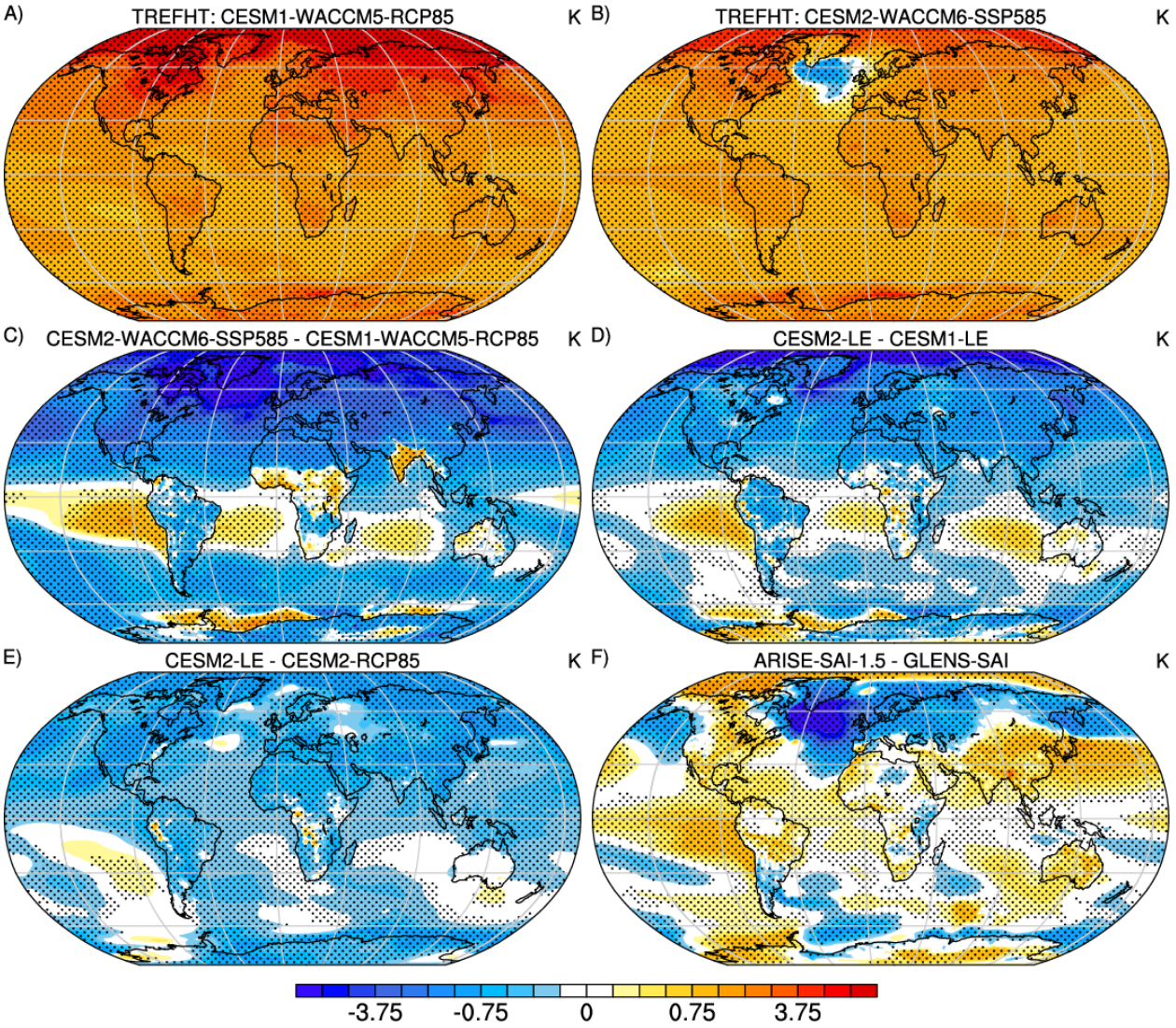

Figure 2. Response in near surface air temperature (TREFHT) estimated from the change between 2020-39 and 2050-69 for unmitigated (a) CESM1-WACCM5-RCP85 and (b) CESM2-WACCM6-SSP585 simulations, and (c) their difference (b-a). Also shown is (d) the analogous difference for the CESM1-LE and CESM2-LE and (e) the CESM2-RCP85 and CESM2-LE. The difference between the geoengineered climate states in ARISE-SAI-1.5 and GLENS-SAI is shown in (f). Units for all panels are K and stippled regions indicate differences that exceed

twice the ensemble standard error.

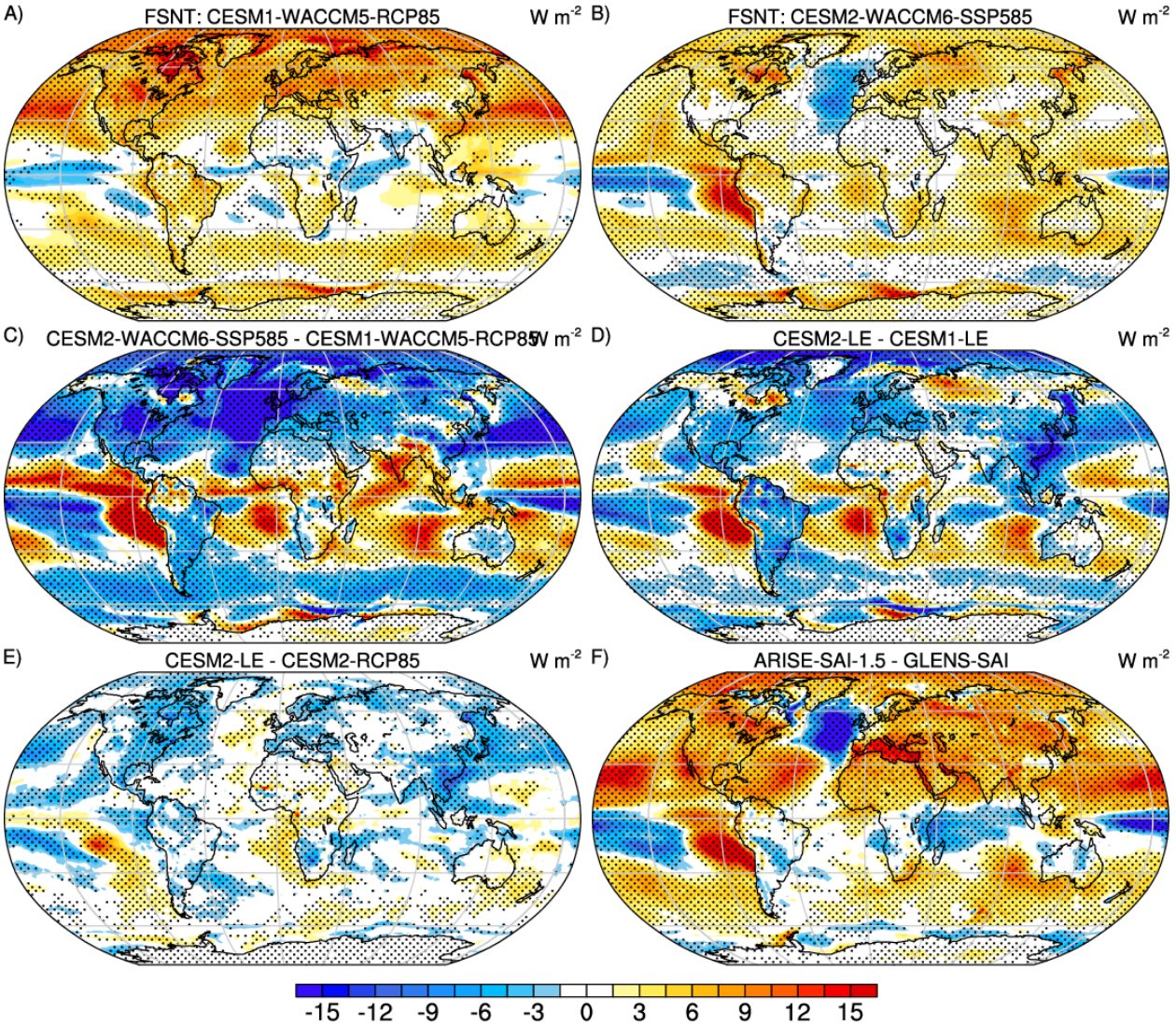

Figure 3. Response in net top-of-atmosphere radiation (FSNT) estimated from the change between 2020-39 and 2050-69 for unmitigated (a) CESM1-WACCM5-RCP85 and (b) CESM2-WACCM6-SSP585 simulations, and (c) their difference (b-a). Also shown is (d) the analogous difference for the CESM1-LE and CESM2-LE and (e) the CESM2-RCP85 and CESM2-LE. The difference between the geoengineered climate states in ARISE-SAI-1.5 and GLENS-SAI is shown in (f). Units for all panels are watts per square meter and stippled regions indicate differences that exceed twice the ensemble standard error.

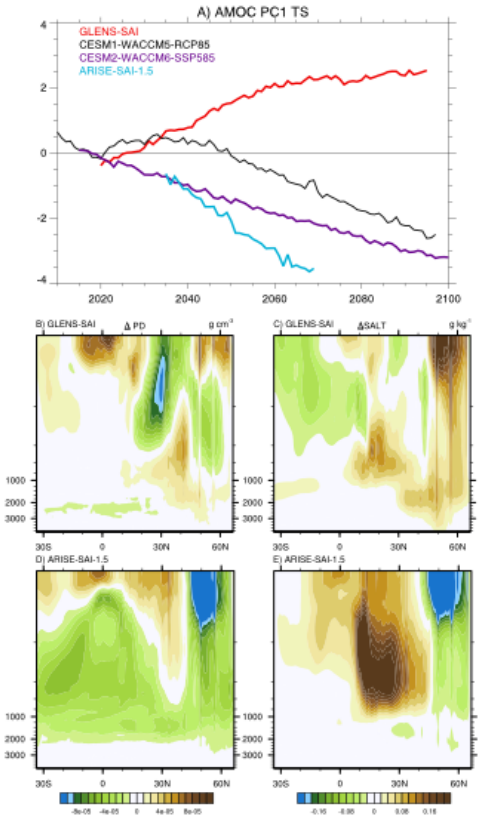

Figure 4. (a) Changes in the leading principal component of the Atlantic Meridional Overturning Circulation in unmitigated (CESM1-WACCM5-RCP85, CESM2-WACCM6-SSP585) and mitigated (GLENS-SAI, ARISE-SAI-1.5) experiments. Also shown are changes in the latitude-depth structure in the Atlantic Ocean of ocean potential density (PD, b, d, units of g cm^{-3}) and salinity (SALT, c, e, units of g kg^{-1}) for GLENS-SAI (b, c) and ARISE-SAI-1.5 (d, e), respectively.

Figure Captions

Figure 1. Evolution of yearly injection mass (Tg SO2 yr^{-1}) over time at the four injection latitudes for (a) GLENS-SAI and (b) ARISE-SAI-1.5 from 2035 to 2070.

Figure 2. Response in near surface air temperature (TREFHT) estimated from

the change between 2020-39 and 2050-69 for unmitigated (a) CESM1-WACCM5-RCP85 and (b) CESM2-WACCM6-SSP585 simulations, and (c) their difference (b-a). Also shown is (d) the analogous difference for the CESM1-LE and CESM2-LE and (e) the CESM2-RCP85 and CESM2-LE. The difference between the geoengineered climate states in ARISE-SAI-1.5 and GLENS-SAI is shown in (f). Units for all panels are K and stippled regions indicate differences that exceed twice the ensemble standard error.

Figure 3. Response in net top-of-atmosphere radiation (FSNT) estimated from the change between 2020-39 and 2050-69 for unmitigated (a) CESM1-WACCM5-RCP85 and (b) CESM2-WACCM6-SSP585 simulations, and (c) their difference (b-a). Also shown is (d) the analogous difference for the CESM1-LE and CESM2-LE and (e) the CESM2-RCP85 and CESM2-LE. The difference between the geoengineered climate states in ARISE-SAI-1.5 and GLENS-SAI is shown in (f). Units for all panels are watts per square meter and stippled regions indicate differences that exceed twice the ensemble standard error.

Figure 4. (a) Changes in the leading principal component of the Atlantic Meridional Overturning Circulation in unmitigated (CESM1-WACCM5-RCP85, CESM2-WACCM6-SSP585) and mitigated (GLENS-SAI, ARISE-SAI-1.5) experiments. Also shown are changes in the latitude-depth structure in the Atlantic Ocean of ocean potential density (PD, b, d, units of g cm^{-3}) and salinity (SALT, c, e, units of g kg^{-1}) for GLENS -SAI(b,c) and ARISE-SAI-1.5 (d,e), respectively.

Figure S1: Response in net top-of-atmosphere radiative flux (RTMT) estimated from the change between 2020-39 and 2050-69 for unmitigated (a) CESM1-WACCM5-RCP85and (b) CESM2-WACCM6-SSP585 simulations, and (c) their difference (b-a). Also shown is (d) the analogous difference for the CESM1-LE and CESM2-LE and (e) the CESM2-RCP85 and CESM2-LE. The difference between the geoengineered climate states in ARISE-SAI-1.5and GLENS-SAI is shown in (f). Units for all panels are W m^{-2} and stippled regions indicate differences that exceed twice the ensemble standard error.

Figure S2: Response in outgoing top-of-atmosphere longwave flux (FLNT) estimated from the change between 2020-39 and 2050-69 for unmitigated (a) CESM1-WACCM5-RCP85 and (b) CESM2-WACCM6-SSP585 simulations, and (c) their difference (b-a). Also shown is (d) the analogous difference for the CESM1-LE and CESM2-LE and (e) the CESM2-RCP85 and CESM2-LE. The difference between the geoengineered climate states in ARISE-SAI-1.5 and GLENS-SAI is shown in (f). Units for all panels are W m^{-2} and stippled regions indicate differences that exceed twice the ensemble standard error.

Figure S3: Response in 4xCO2AMIP of top-of-atmosphere outgoing shortwave radiation (W m^{-2}) in (a) CESM1, (b) CESM2, and (c) the difference (b-a).

Figure S4: Rapid adjustments of cloud amount (%) to CO_2 based on 4xCO2AMIP-AMIP simulation differences in (a) CESM1, (b) CESM2, and (c) their difference (b-a).

Figure S5: Response in 4xAbruptCO2 simulations of TOA outgoing shortwave radiation for (a) CESM1, (b) CESM2, and (c) their difference. Also shown are associated timeseries of hemispheric mean fluxes (d) and their differences (e).

Figure S6: Response in surface salinity estimated from the change between 2020-39 and 2050-69 for unmitigated (a) CESM1-WACCM5-RCP85 and (b) CESM2-WACCM6-SSP585 simulations, and their difference (c). Also shown is the analogous difference for (d) the CESM1-LE and CESM2-LE (d) and (e) the CESM2-RCP85 and CESM2-LE. The difference between the geoengineered climate states in ARISE-SAI-1.5 and GLENS-SAI is shown in (f).

Figure S7: Rapid adjustments of precipitation (mm day^{-1}) to CO_2 based on 4xCO2AMIP-AMIP simulation differences in (a) CESM1, (b) CESM2, and (c) their difference (b-a).

Figure S8: Response in sulfate aerosol burdens (BURDENSO4dn) estimated from the change between 2020-39 and 2050-69 for unmitigated (a) CESM1-WACCM5-RCP85 and (b) CESM2-WACCM6-SSP585 simulations, and (c) their difference (b-a). Also shown is (d) the analogous difference for the CESM1-LE and CESM2-LE and (e) the CESM2-RCP85 and CESM2-LE. The difference between the geoengineered climate states in ARISE-SAI-1.5 and GLENS-SAI is shown in (f). Units for all panels are W m^{-2} and stippled regions indicate differences that exceed twice the ensemble standard error. The difference field in (f) is scaled by $1/5^{\text{th}}$.